



# CHORUS

This is the accepted manuscript made available via CHORUS. The article has been published as:

## Crystallization of $^4\text{He}$ in aerogel via mass flow from surrounding solid $^4\text{He}$

H. Matsuda, A. Ochi, R. Isozaki, S. Minami, R. Nomura, J. Pollanen, W. P. Halperin, and Y. Okuda

Phys. Rev. B **94**, 024509 — Published 14 July 2016

DOI: [10.1103/PhysRevB.94.024509](https://doi.org/10.1103/PhysRevB.94.024509)

# Crystallization of $^4\text{He}$ in Aerogel via Mass Flow from Surrounding Solid $^4\text{He}$

H. Matsuda<sup>1</sup>, A. Ochi<sup>1</sup>, R. Isozaki<sup>1</sup>, S. Minami<sup>1</sup>, R. Nomura<sup>1,\*</sup>, J. Pollanen<sup>2†</sup>, W. P. Halperin<sup>2</sup>, and Y. Okuda<sup>1†</sup>

<sup>1</sup>*Department of Physics, Tokyo Institute of Technology, Meguro, Tokyo 152-8551, Japan and*

<sup>2</sup>*Department of Physics and Astronomy, Northwestern University, Evanston, Illinois 60208, USA*

(Dated: June 28, 2016)

The phase boundary between the quantum solid and liquid phases of  $^4\text{He}$  is strongly modified in a porous material. However the phase diagram at very low temperatures remains unexplored. We have used a variable-volume experimental cell with optical access to visualize the crystallization of  $^4\text{He}$  in silica aerogels with independent control of the pressure and temperature. The onset of crystallization was investigated in two aerogel samples with differing porosity both by pressurization at constant temperature and by cooling at constant pressure. With isothermal pressurization we have established a low temperature phase diagram for each aerogel and we find that the equilibrium crystallization pressure is reduced with increasing aerogel porosity. Crystals also began to grow in the aerogel on cooling at fixed pressure below an onset temperature,  $T_{grow}$ . We found that below this temperature the crystallization rate increased with decreasing temperature. The aerogel in our cell was surrounded by bulk crystals of  $^4\text{He}$  and surprisingly  $T_{grow}$  was found to be widely distributed when the surrounding bulk crystals were repressurized. In this experimental arrangement, crystallization within the aerogel on cooling requires mass flow from these exterior bulk crystals and is strongly influenced by the disordered structure at the interface between the bulk solid and the helium within the aerogel.

PACS numbers: 67.80.bd, 67.80.bf, 67.25.D-, 64.70.D-

## I. INTRODUCTION

$^4\text{He}$  in porous media is an ideal system to investigate the phase transition dynamics in the presence of quenched disorder. Crystallization of  $^4\text{He}$  is especially intriguing because the low temperature environment is free from impurities [1, 2] and the superfluid can flow swiftly through pores which allows reproducible observation of crystallization on short time scales [3–7] that is hardly realized in classical systems [8]. In the present work we have taken advantage of this approach to perform a visualization study of crystallization in two samples of high porosity silica aerogel with different density with independent control of temperature and pressure. The crystallization we observed depends on mass transport into the superfluid phase within the aerogel from the bulk solid  $^4\text{He}$  that completely encloses it. This subject is of substantial current interest in the context of possible supersolidity in  $^4\text{He}$ . In recent experiments [9–12] mass flow was reported between bulk solid helium and the superfluid in a porous medium, Vycor glass.

Following torsional oscillator experiments on solid  $^4\text{He}$  by Kim and Chan [13, 14], the existence of a supersolid phase has been a hotly debated topic in condensed matter physics. Subsequent works revealed elastic stiffening of the  $^4\text{He}$  solid in the same temperature range [15], and thus the torsional oscillator anomaly was re-interpreted in view of the mechanical responses of the  $^4\text{He}$  crystals. Using a “flow-standpipe” arrangement, Hallock and coworkers [9–11] observed mass flow through solid  $^4\text{He}$  that has been interpreted as an indication of supersolid-

ity. Recently, however, this scenario was questioned by Cheng *et al* [12], based on their experiment of mass flow through a solid-superfluid-solid junction. Since mass flow in solid  $^4\text{He}$  is not yet fully understood it is important to develop complementary experimental approaches for mass flow measurement to provide new insights. In the present work we pursue a new direction by examining how crystallization proceeds in highly porous silica aerogel and how it relates to mass flow from surrounding bulk crystals.

The density of solid  $^4\text{He}$  is greater than that of the liquid; therefore, crystallization in a porous medium is inevitably accompanied by mass flow to compensate for the density difference as long as the volume is constant. In our experiment this process can be visualized and is necessarily influenced by the mechanism for mass transport from the surrounding bulk crystals. In previous work, crystallization of  $^4\text{He}$  in pores has been studied extensively using the method of a blocked fill capillary at high temperatures [16–19]. However, this approach does not work at very low temperatures where the phase diagram details are unknown and the mechanism for mass transport in the bulk solid phase remains an open question. Our experimental arrangement is specifically designed to explore this region.

We have measured the critical pressure for nucleation of solid helium in both of our aerogel samples as a function of temperature and have studied crystallization above this limiting pressure. On cooling at constant pressure we find that  $^4\text{He}$  crystal growth starts at a well-defined onset temperature,  $T_{grow}$ , a process that requires mass to flow into the aerogel superfluid. Our observations of the existence of an onset temperature for crystal growth are reasonably consistent with previous reports for the onset of mass flow in bulk  $^4\text{He}$  solid. We have

---

\* nomura.r.aa@m.titech.ac.jp

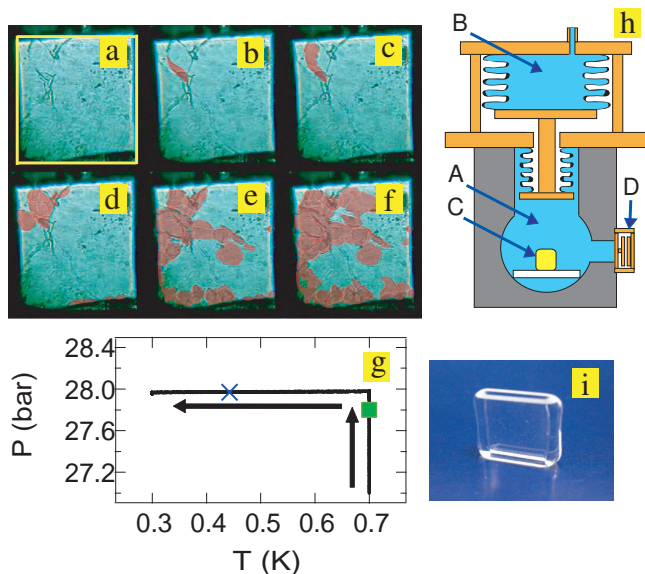


FIG. 1. (color online) a-f: Images of the crystallization process in the 96% porosity aerogel at (a, b) 0.70, (c) 0.44, (d) 0.31, and (e, f) 0.30 K. The width of each picture is 10 mm. The frame shown in (a) indicates the aerogel. Painted (red) areas represent the crystallized regions. (g): Temperature-pressure trace measured during the crystallization process. The square indicates the pressure,  $P_c$ , at which crystals were first nucleated. During a temperature sweep at a slightly higher pressure, the start of crystal growth on cooling was observed at,  $T_{grow}$ , shown by the symbol x. (h): Schematic of the variable-volume cell. (i): Image of the glass aerogel sample holder.

studied this process under controlled circumstances in two rather different aerogel samples, finding that  $T_{grow}$  depends on the nature of the porous medium and is limited by mass flow from the surrounding bulk solid  $^4\text{He}$ .

## II. EXPERIMENTAL SETUP

Silica-aerogel is a highly porous material with good optical transparency, consisting of nanometer-scale, silica particles connected in a fractal-like structure [20–22]. The effects of aerogel on the condensed phases of helium have been widely investigated [5–7, 19, 22–29] making this material a paradigm for the study of quenched disorder on quantum fluid and solid phases.

For our experiments, aerogel samples with porosities of 96% and 98% were grown via a standard sol-gel technique [30] *in situ* in glass sample holders having rectangular dimensions of  $1 \times 8 \times 10 \text{ mm}^3$  as shown in Fig. 1(i). The aerogel samples did not shrink during growth and there was no gap between the inner wall of the glass and the aerogel. The lower aperture of the glass sample holder was glued to a glass plate to ensure that the aerogel inside had contact with the external environment only through

the upper aperture. A  $^4\text{He}$  sample with a nominal concentration of a few hundred parts per billion (ppb)  $^3\text{He}$  was used in all the experiments reported here[31]. Impurities of this concentration cannot have a severe influence on the mass transport in our experimental temperature range[32].

Experiments were conducted in a dilution refrigerator with optical windows for visualization of the crystallization processes [6, 7]. A variable-volume cell was used: Fig. 1(h), comprised of two chambers, a high-pressure chamber (A) and a low-pressure chamber (B), to address the difficulties of the blocked capillary method. Different diameter phosphor bronze bellows were connected by a rigid copper rod permitting pressurization of the helium in the aerogel in order to observe crystallization at pressures above the bulk crystallization curve. The aerogel (C) was placed in chamber (A), the volume of which was controlled by pressurization of the liquid helium in chamber (B). A capacitive pressure gauge (D) was installed on the side wall of chamber (A), 20 mm away from the center of the aerogel, and the pressure  $P$  of the bulk crystals outside the aerogel was measured through a 5 mm diameter, 6.9 mm long hole. The temperature  $T$  of the bulk crystal was measured directly with a calibrated  $\text{RuO}_2$  thermometer in chamber (A). Chamber (A) had optical windows to observe the crystallization processes from outside the refrigerator. With this experimental cell independent control of  $P$  and  $T$  was achieved over a wide range of the phase diagram enabling us to grow, via pressurization, a desired amount of solid helium in the aerogel prior to sweeping the temperature as shown in Fig. 1 (g) [33]. In our previous work, using the same apparatus and by pressurizing at constant temperature, we demonstrated that  $^4\text{He}$  crystallizes in aerogel via creep at high temperatures and via avalanches at low temperatures [5–7].

## III. RESULTS

In the present work we investigate the temperature dependence of the crystal growth in aerogel. Initially the aerogel was filled with superfluid surrounded by solid helium, shown in Fig. 1(a) for the 96% porosity aerogel at 25.6 bar, well above the crystallization pressure of the bulk solid but below the crystallization pressure in the aerogel. Chamber (A) was compressed to increase  $P$  while keeping the temperature constant at  $T = 0.70$  K. Crystals nucleated in the aerogel at a critical pressure of  $P_c = 27.8$  bar indicated by the green square in Fig. 1(g) and pressurization was stopped at  $P = 27.98$  bar at which time the crystals (shown in red) stopped growing and coexisted with the liquid in the aerogel, Fig. 1(b). Thereafter, the system was cooled at a uniform rate of approximately 10 mK/min during which time the amount of solid helium in the aerogel did not change until a temperature  $T_{grow}$  was reached. For the particular experiment shown in Fig. 1(g) this corresponds to 0.44 K. Below this temperature crystals grew via intermittent local nucle-

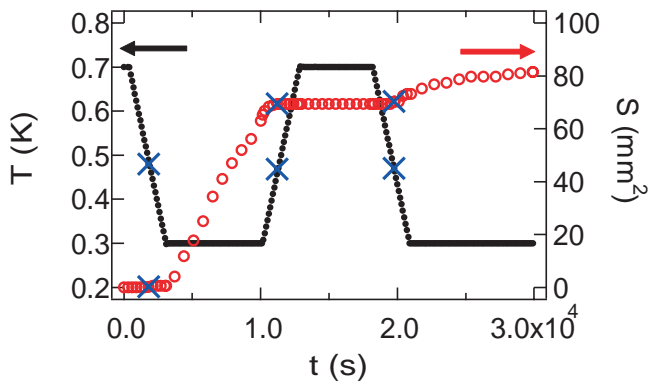


FIG. 2. (color online) The amount of crystals  $S$  in the 96% porosity aerogel as a function of time during the cooling and warming temperature sweeps following an initial pressurization to  $P = 27.85$  bar. The x-symbols indicate the temperature  $T_{grow}$  at which crystallization began with cooling and stopped with warming. Although  $S$  seems to increase near  $t = 3 \times 10^3$  s, in fact  $S$  started to increase at  $1.8 \times 10^3$  s, clearly resolved optically.

ation [34], a phenomenon that we refer to as avalanches [5–7], which can be seen in the video clip of the cooling process [35]. Upon further cooling, the crystals continued to grow (Fig. 1c-f) until they finally filled the entire aerogel sample. This video provides a direct visualization of the crystallization process and the concomitant mass flow from the surrounding solid  $^4\text{He}$  that encloses the aerogel. It is important to note that during crystallization on cooling the volume change of the aerogel sample containing liquid and solid helium was observed optically to be less than 1%. The volume change from the known compressibility of both helium and aerogel [29, 36, 37] is less than 0.05%. Since these are less than the density difference between liquid and solid, of order 10%, our observations are consistent with mass flow into the aerogel sample.

Our observations of crystallization during cooling and warming temperature sweeps are presented as a function of time in Fig. 2. The amount of crystal in the aerogel,  $S$ , is given by the projected area of the crystal, which is determined visually. A small amount of crystalline helium coexisted with the liquid in the aerogel for the initial conditions at  $T = 0.70$  K and  $P = 27.85$  bar. On cooling,  $S$  began to increase at a temperature  $T_{grow} = 0.480$  K, indicated by the x-symbols in the figure, and continued to increase without stopping even when the temperature was kept constant at  $T = 0.3$  K. Thereafter, the system was warmed up and  $S$  stopped increasing at  $T = 0.468$  K, very close to  $T_{grow}$ . On cooling once again,  $S$  began to increase at the temperature  $T = 0.470$  K, again very close to  $T_{grow}$ . During this temperature sweep experiment the amount of solid helium in the aerogel is transient and the system is out of equilibrium. Although the equilibrium state would have the aerogel completely filled with solid we increased the temperature and stopped crystal-

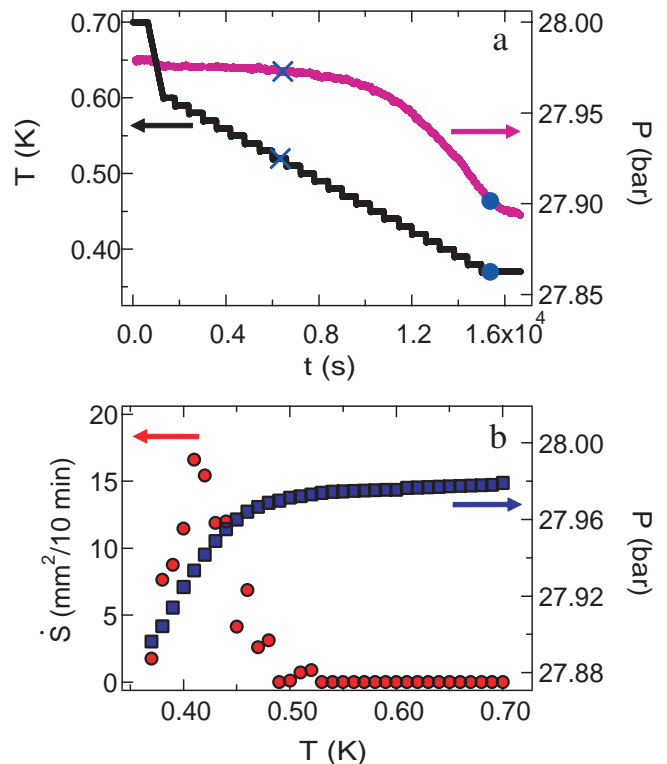


FIG. 3. (color online) (a): Traces of temperature and pressure for the surrounding bulk crystals as a function of time for 10 mK, stepwise-cooling at 10 minute intervals. The x-symbols and solid circles are the beginning and the completion of crystallization in the 96% porosity aerogel during cooling. (b): Growth rate of crystals and pressure as a function of temperature for the procedure in (a). Note that time runs to the left in (b) on cooling.

lization before this state was reached. We are able to observe this transient process because the crystallization rate is finite as will be discussed shortly. From the data in Fig. 2 it is clear that the onset of crystal growth is rather sharp, reproducible, and non-hysteretic to an accuracy of a few percent spanning a wide range in the total amount of solid filling the aerogel. Consequently the onset temperature for crystal growth is completely determined by intrinsic properties of the aerogel and the configuration of the solid  $^4\text{He}$  that surrounds it. We will return to this important observation later in the discussion to contrast it with the wide distribution of  $T_{grow}$  after much larger pressure changes in the cell.

To investigate the rate of crystallization, the system was cooled in 10 mK steps after which temperature was held constant for 10 min following each step as shown in Fig. 3(a). These temperature steps were sufficient to ensure thermal equilibrium within the sample. After the onset of crystallization corresponding steps in the pressure are not observed due to the fact that crystallization continues within the aerogel even after the temperature has equilibrated. The x-symbols and circles indicate

the points at which the crystallization process started and was completed. The increase of  $S$  during each 10 min holding period was measured during each step from which the growth rate  $\dot{S}$  was determined. Data for a representative growth measurement of the growth rate is shown as a function of temperature in Fig. 3(b) along with the measured pressure. From the experiment in Fig. 3(b), at  $T < T_{grow} = 0.52$  K, we found that  $\dot{S}$  gradually increased on cooling and then decreased below 0.41 K while the pressure decreased continuously throughout, although markedly faster at lower temperatures.

The temperature dependence of  $\dot{S}$  in Fig. 3(b) shows a gradual increase on cooling similar to the mass flow rates in solid  $^4\text{He}$  reported recently by others [10–12], although their measured onset temperatures were higher. The mass flow rate estimated from our measurements of  $\dot{S}$  are in rough agreement with those reported in Ref. [32]. These similarities suggest that these different experiments have a common basis and we infer that the crystal growth rate in aerogel is dependent in some manner on the mass flow from the surrounding solid. One difference with what has been previously reported however, is that we find  $\dot{S}$  to decrease below 0.41 K. However, because the pressure in our cell also decreased in this low temperature region, we expect that the driving force for crystallization will be smaller accounting for this drop in  $\dot{S}$ .

Different crystallization behavior in the 96% and 98% aerogels was observed as is evident in the  $P$ - $T$  diagram of Fig. 4. Upper and lower data sets are for the 96% and 98% porosity aerogels, respectively, and can be compared with the bulk crystallization pressure [36] given by the solid curve. First, we determined the equilibrium critical pressure-temperature phase diagram,  $P_c(T)$ , where  $P_c$  is the pressure at which the first crystals were nucleated in the aerogel while pressurizing at constant temperature, as previously described [7]. Our procedure was to fill the aerogel with liquid and form solid outside the aerogel, compressing the helium in chamber (A) by pressurizing chamber (B) while keeping  $T$  constant. The pressure at which crystals nucleated in the aerogel identified  $P_c$  and thereafter they continued to grow. Then chamber (A) was decompressed in order to decrease  $P$ , melting the crystals in the aerogel, keeping the pressure above the crystallization pressure for the bulk solid. This procedure was repeated at various  $T$  to determine the temperature dependence of  $P_c(T)$  shown as green squares in Fig. 4. For the 96% porosity aerogel,  $P_c$  was approximately 27.2 bar at temperatures below 0.5 K and was found to have an anomalous maximum of  $P_c \approx 27.8$  bar at 0.7 K. For the 98% porosity aerogel,  $P_c$  was almost temperature independent at low temperature and decreased slightly above 0.6 K [7]. In both aerogels, the crystals grew via creep or avalanches depending on temperature [5–7]. A pressure of approximately 0.3 bar above  $P_c$  is sufficient to completely crystallize the liquid in the aerogel (violet diamonds). These measurements establish the equilibrium phase diagram and an experimental window of pressure

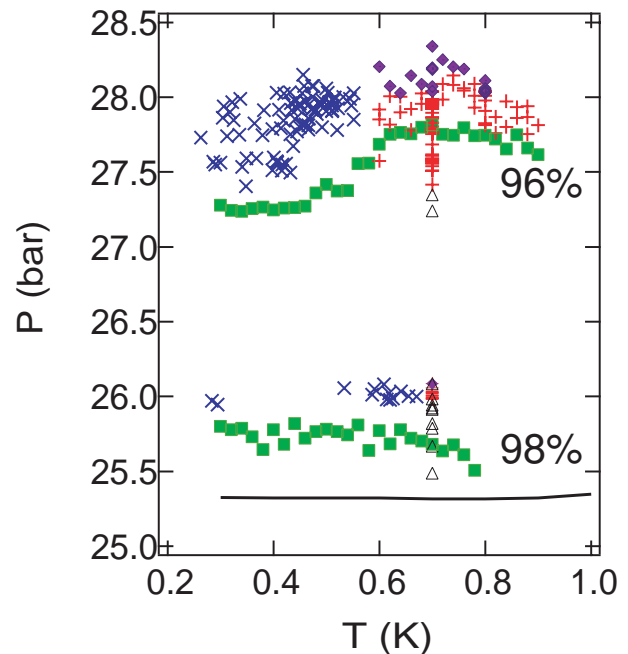


FIG. 4. (color online) Temperature-pressure diagram for crystallization in 96% (upper data) and 98% (lower data) porosity aerogels. Green squares are the critical nucleation pressures  $P_c$  in pressurization at constant temperature. Blue x-symbols indicate the starting temperature for crystal growth  $T_{grow}$  on cooling from initial conditions given by red crosses at  $T_i$ . Black triangles are the initial conditions under which no crystal formed. Violet diamonds indicate conditions where crystal growth continued until completion. The solid curve is the bulk crystallization pressure.

for examination of crystallization on cooling.

In Fig. 4, we also present our cooling measurements of  $T_{grow}$  from various initial conditions, which were prepared by pressurization from an initial temperature,  $T_i$ . This protocol allowed us to produce a small amount of crystals in the aerogel with  $P > P_c$  or, alternatively, with only liquid present in the aerogel with  $P < P_c$ . These initial points at various  $P$  and  $T_i$  are indicated by the red crosses or black triangles prior to cooling at constant pressure. The red crosses correspond to initial conditions for which crystals started to grow at the onset temperature  $T_{grow}$ , which are marked by blue crosses. Black triangles indicate that crystals never formed down to our lowest temperature, 0.21 K. After each cooling run the aerogel solid was melted by depressurizing to about 26.0 bar for the 96% aerogel. The cell was then warmed, pressurized to establish new initial conditions, and the cooling experiment was repeated. For both aerogel samples  $T_{grow}$  was found to be widely distributed. There was no apparent correlation between  $T_{grow}$  and the initial temperature  $T_i$  as shown in Fig. 5 for the 96% aerogel. Nonetheless, the points  $P(T_{grow})$  generally followed the behavior of the critical pressure  $P_c(T)$  as can be seen in Fig. 4. We draw attention to the upper-bound of the

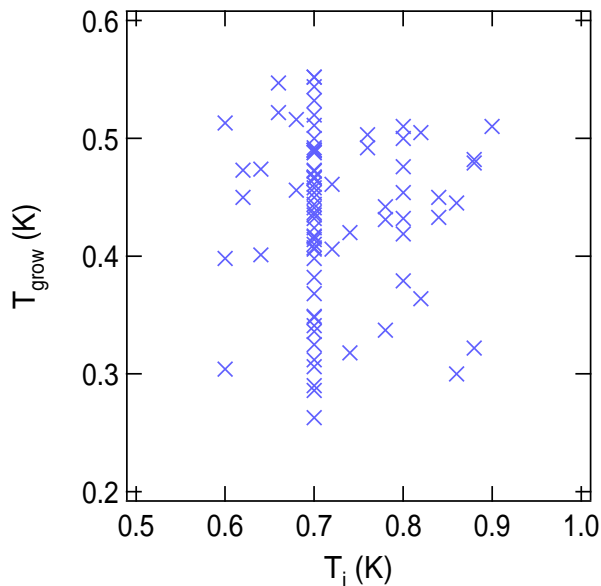


FIG. 5. (color online)  $T_{grow}$  shown in Fig. 4 as a function of the initial temperature before cooling,  $T_i$ , for the 96% aerogel. There was no apparent correlation between  $T_{grow}$  and  $T_i$ .

distribution of  $T_{grow}$  noting that this is much higher for the 98% aerogel. Crystals did not always form by cooling in the 98% aerogel even when some amount of crystals were initially present as indicated by the black triangles above the low temperature limit of  $P_c$ .

## IV. DISCUSSION

### A. Crystallization

Some of the intrinsic features for the crystallization in the aerogel, not seen in the bulk  $^4\text{He}$ , are apparent in Fig. 4. One is the history dependence which is often observed in phase transitions in the presence of disorder. The onset of crystallization between the two types of experiments, by pressurization at constant temperature or by cooling at constant pressure, are indeed different. Secondly, solidification on cooling is very unusual in view of the extensively studied crystallization of bulk  $^4\text{He}$  [1, 2] when solid and superfluid coexist on the equilibrium crystallization pressure-temperature curve. In this case crystals never grew on cooling at low temperatures because the equilibrium crystallization pressure is nearly temperature independent. Overpressure is the only driving force for crystallization and cooling should have a minimal influence on crystallization [33]. Therefore, both the history dependence and crystallization on cooling are intrinsic features of solidification in aerogel, revealed in the present experiment owing to our capabil-

ity to independently control pressure and temperature in the unexplored low temperature region.

Furthermore, two conditions must be satisfied for crystallization to proceed in aerogel. First, mass must be supplied to the aerogel from the outer bulk solid, and secondly the crystal phase in the aerogel must be stable.

We infer from the pressure, and sample, dependence for the onset of crystal growth and from the stochastic character of  $T_{grow}$  that crystallization is a nucleation phenomenon controlled by the aerogel structure. It is important to note that this type of stochastic behavior has not been observed in the experiments with Vycor glass [9–12]. At first sight the wide distribution of  $T_{grow}$  might appear to be at odds with our observation during a single cooling or warming experiment, as in Fig. 2, that  $T_{grow}$  is very well-defined and independent of the solid content  $S$  in the aerogel, from which it is clear that the crystals within the aerogel are stable. However, an essential difference between the experiments of Fig. 2 and Fig. 4 is that from one cooling run to another, as represented in Fig. 4, the surrounding solid is modified before each experiment by pressure changes of several bar in contrast with the single cooling experiment in Fig. 2 where pressure changes are more than an order of magnitude smaller. Taken together, these results show that the mechanism for mass transport from the bulk solid into the aerogel is modified in an uncontrolled way by differences produced by pressurization of the bulk solid that take place between the various cooling runs, resulting in a wide distribution of  $T_{grow}$ . It is reasonable to associate this stochastic nature of  $T_{grow}$ , from one pressurization to the next, with the disordered interface between the aerogel and the bulk solid since a distribution in the onset temperature for mass flow has not been observed in any of the other experiments reporting flow in solid  $^4\text{He}$ .

### B. Mass Transport

As noted previously, for the crystallization in aerogel to occur, mass supply is needed from the outer bulk solid to compensate for the density difference between the liquid and solid. This mass flow can be separated into two serial processes: how the atoms enter the aerogel at the upper aperture and how these  $^4\text{He}$  atoms in the bulk crystal come to the aperture of the aerogel. In the case of the pressurization experiment at constant temperature, there are two possibilities for how helium enters the aerogel: solid melting at the aerogel aperture or penetration of the solid into the pores via plastic deformation as proposed in our earliest publication, Ref. [5]. In a later publication, Ref. [6], in which aerogel in a glass tube was used to elucidate how atoms enter aerogel, penetration of the solid was excluded because liquid always existed between the crystals in the aerogel and the outer bulk solid so that the solid melted at the aerogel aperture under stress and entered the aerogel in the liquid state. In the case of cooling at nearly constant pressure,  $^4\text{He}$

atoms similarly must have entered aerogel in the liquid state since the crystals in the aerogel formed away from the aperture with minimal contact to the bulk solid as shown in Fig. 1.

It is also important to understand how the  $^4\text{He}$  atoms come from the bulk solid to the aperture, in order to keep supplying  $^4\text{He}$  atoms for crystallization in the aerogel. In the case of the pressurization experiment, atoms can simply move toward the aperture because the solid is mechanically compressed toward the aerogel by the bellows (Fig. 1h) and experience plastic deformation. In contrast during the cooling experiments, without compression mass flow is needed from the outer bulk solid. In this case three possible mechanisms for mass flow have been proposed [9–12, 38, 39]; (i) along dislocation cores, (ii) along superfluid layers between a wall and crystal, and (iii) flow driven by the relaxation of residual strain in the bulk solid from plastic deformation. In the following we examine our results in the context of these three possibilities for bulk mass flow

The total mass flow rate into the aerogel from the exterior bulk region  $\dot{m}$  can be estimated from our measurements of the crystal growth rate. To convert  $\dot{S}$  in Fig. 3 to the rate of increase of the crystal volume  $\dot{V}$ , or to the  $\dot{m}$  into the aerogel, the approximate expression  $\dot{S}d \approx \dot{V} = \dot{m}/(\rho_s - \rho_l)$  can be used, where  $d = 1$  mm is the aerogel thickness and  $\rho_s$  and  $\rho_l$  are the respective densities of the solid and liquid. A typical value of  $\dot{S} = 10$  mm<sup>2</sup>/10 min in Fig. 3 corresponds to  $\dot{m} \approx 2 \times 10^{-7}$  g/s. Similar values of the mass flow rate were reported by the direct flow measurement in bulk solids in Ref. [32]. Since the cross section of the flow channel cannot be largely different in these two experiments of similar dimension, their mass flux should also be of the same order of magnitude, supporting that the crystal growth rate is determined by the mass flow rate from the surrounding solid helium outside the aerogel.

After the helium inside the aerogel is completely crystallized the pressure drop outside can be estimated to be  $\Delta P = (\rho_s - \rho_l)\phi V_1/\rho_s \kappa V_2 \approx 0.1$  bar. Here,  $\phi$ ,  $V_1 = 80$  mm<sup>3</sup>,  $V_2 \approx 18$  cm<sup>3</sup> and  $\kappa = 3.7 \times 10^{-3}$  bar<sup>-1</sup> are the porosity, volume of the aerogel, volume of chamber (A), and compressibility of the crystal, respectively [36].  $\Delta P$  is consistent with the observed drop of  $P$  in Fig. 3, which supports the idea of a nearly uniform supply of mass from the surrounding solid.

We first discuss flow scenarios (i) and (ii). If the mass is transported by the superfluid through  $N$  channels with cross-section  $A$  at a critical velocity  $v_c$ , then  $\dot{m} = N\xi A\rho_l v_c$ , where  $\xi$  is the condensate fraction. It was theoretically predicted that the core of dislocations in  $^4\text{He}$  crystals can support superflow [38, 40]. For case (i), the number of dislocations through the aperture can be estimated to be  $N \approx 1 \times 10^7$  using  $\dot{m} \approx 2 \times 10^{-7}$  g/s, when  $A = 1$  nm<sup>2</sup>,  $\xi = 1$  and  $v_c \approx 10$  cm/s. This value corresponds to a dislocation line density of  $\Lambda \approx 3 \times 10^8$  cm<sup>-2</sup>, which is smaller than one previously reported [41], but is two orders of magnitude larger than another more

recently reported value [42]. Considering case (ii) where mass transport is attributed to superfluid layers on the wall of 1 nm thickness. An estimate of  $\dot{m}$  that is consistent with our measurements of  $\dot{S}$  can be obtained by setting  $N = 1$  and  $A = 1$  nm  $\times$  10 mm. Consequently, based on our measurements, these two processes for mass flow are both plausible but cannot be distinguished. However, we note that the mechanism by which helium atoms are transported to either dislocation lines or to a superfluid phase at the wall remain open questions which have not been satisfactorily addressed by any of the experiments to date.

Next, we address scenario (iii) where the mechanism for transport is produced by the relaxation of residual plastic deformation in the solid. This mechanism will be governed by the strain distribution in the bulk solid as well as its geometry, neither of which are known and therefore our experiments can neither confirm nor deny its existence. To identify, or conversely rule out, this mechanism one should design an experiment in which the strain configuration of the solid is systematically varied. In this regard we emphasize that in all previous experiments, including our own, mechanism (iii) has not been ruled out.

Finally, null results of mass flow have been reported in some transport experiments [43–45]. The origin of this discrepancy has not yet been clarified; however, there was no superfluid present in the experiments producing null flow results. In contrast there are significant amounts of superfluid liquid in the present work and in that of Hallock *et al.* and Cheng *et al.* [9–12]. Regardless of the ultimate flow mechanism, it seems likely that presence of superfluid liquid somewhere in the system is essential for the activation of mass transport. Since the null result experiments were performed at higher pressures, another possibility is that the region of mass transport through solid is confined to a narrow band of pressure close to the equilibrium crystallization pressure below about 28 bar.

## V. SUMMARY

The crystallization of  $^4\text{He}$  in aerogels was investigated visually with independent control of the pressure and temperature using a variable-volume cell. This allowed us to construct a pressure-temperature phase diagram at low temperatures in two samples of silica aerogel with different porosity. Crystallization in the disordered aerogel medium was found to be induced not only by pressurization at constant temperature but also by cooling at constant pressure. On cooling, this solidification only occurred below a temperature  $T_{grow}$  that requires mass to be transferred from the surrounding bulk solid into the aerogel to compensate for the density difference between liquid and solid. This onset for mass flow var-

ied widely with different pressurizations of the bulk solid and appears to be limited by a process at the interface between the bulk solid and the aerogel. Our measurements indicate the important role of this interface in the crystallization of helium in aerogel. However, while our results require helium mass transport of the bulk solid to that interface we have not determined the transport mechanism.

## VI. ACKNOWLEDGEMENT

This study was supported in part by the GCOE at Tokyo Tech. “Nanoscience and Quantum Physics

Project”, a Grant-in-Aid for Scientific Research (B) (No. 26287074) from MEXT Japan, a “Ground-based Research Announcement for Space Utilization” promoted by JAXA, the Hosokawa Powder Technology Foundation, Toyota Physical & Chemical Research Institute, and by the National Science Foundation grant No. DMR-1103625.

<sup>†</sup>Present address: RIKEN CEMS, 2-1 Hirosawa, Wako-shi, Saitama 351-0198, Japan.

<sup>‡</sup> Present address: Department of Physics and Astronomy, Michigan State University, East Lansing, Michigan 48824, USA.

- 
- [1] S. Balibar, H. Alles, and A. Ya. Parshin, *Rev. Mod. Phys.* **77**, 317 (2005).
- [2] Y. Okuda and R. Nomura, *J. Phys. Soc. Jpn.* **77**, 111009 (2008).
- [3] T. Mizusaki, R. Nomura, and M. Hiroi, *J. Low Temp. Phys.* **149**, 143 (2007).
- [4] M. Hiroi, T. Mizusaki, T. Tsuneto, A. Hirai, and K. Eguchi, *Phys. Rev. B* **40**, 6581 (1989).
- [5] R. Nomura, A. Osawa, T. Mimori, K. Ueno, H. Kato, and Y. Okuda, *Phys. Rev. Lett.* **101**, 175703 (2008).
- [6] R. Nomura, H. Matsuda, R. Masumoto, K. Ueno, and Y. Okuda, *J. Phys. Soc. Jpn.* **80**, 123601, (2011).
- [7] H. Matsuda, A. Ochi, R. Isozaki, R. Masumoto, R. Nomura, and Y. Okuda, *Phys. Rev. E* **87**, 030401(R) (2013).
- [8] J. G. Dash, A.W. Rempel, and J. S. Wettlaufer, *Rev. Mod. Phys.* **78**, 695 (2006).
- [9] M. W. Ray and R. B. Hallock, *Phys. Rev. Lett.* **100**, 235301 (2008).
- [10] M. W. Ray and R. B. Hallock, *Phys. Rev. Lett.* **105**, 145301 (2010).
- [11] Ye. Vekhov and R. B. Hallock, *Phys. Rev. Lett.* **109**, 045303 (2012).
- [12] Z. G. Cheng, J. Beamish, A. D. Fefferman, F. Souris, S. Balibar and V. Dauvois, *Phys. Rev. Lett.* **114**, 165301 (2015).
- [13] E. Kim and M. H. W. Chan, *Science* **305**, 1941 (2004).
- [14] E. Kim and M. H. W. Chan, *Nature (London)*, **427**, 225 (2004).
- [15] J. Day and J. R. Beamish, *Nature (London)*, **450**, 853 (2007).
- [16] E. D. Adams, K. Uhlig, Y.-H. Tang, and G. E. Haas, *Phys. Rev. Lett.* **52**, 2249 (1984).
- [17] J. R. Beamish, A. Hikata, L. Tell, and C. Elbaum, *Phys. Rev. Lett.* **50**, 425 (1983).
- [18] K. Yamamoto, Y. Shibayama, and K. Shirahama, *J. Phys. Soc. Jpn.* **77**, 013601 (2008).
- [19] K. Matsumoto, H. Tsuboya, K. Yoshino, S. Abe, H. Tsujii, and H. Suzuki, *J. Phys. Soc. Jpn.* **78**, 034601 (2009).
- [20] T. M. Haard, G. Gervais, R. Nomura, and W. P. Halperin, *Physica B* **284**, 289 (2000).
- [21] F. Detcheverry, E. Kierlik, M. L. Rosinberg, and G. Tarjus, *Phys. Rev. E* **68**, 061504 (2003).
- [22] W. P. Halperin, H. Choi, J. P. Davis, and J. Pollanen, *J. Phys. Soc. Jpn.* **77**, 111002 (2008).
- [23] J. Yoon, D. Sergatskov, J. Ma, N. Mulders, and M. H. W. Chan, *Phys. Rev. Lett.* **80**, 1461 (1998).
- [24] R. Nomura, W. Miyashita, K. Yoneyama, and Y. Okuda, *Phys. Rev. E* **73**, 032601 (2006).
- [25] P. Spathis, A. Delga, C. Malheiro, and P. E. Wolf, *J. Low Temp. Phys.* **171**, 693 (2013).
- [26] T. Lambert, C. Gabay, L. Puech, and P. E. Wolf, *J. Low Temp. Phys.* **134**, 293 (2004).
- [27] N. Mulders, J. T. West, M. H. W. Chan, C. N. Kodituwakku, C. A. Burns, and L. B. Lurio, *Phys. Rev. Lett.* **101**, 165303 (2008).
- [28] P. E. Wolf, F. Bonnet, L. Guyon, T. Lambert, S. Perraud, L. Puech, B. Rousset, and P. Thibault, *Eur. Phys. J. E* **28**, 183 (2009).
- [29] T. Herman, J. Day, and J. Beamish, *Phys. Rev. B* **73**, 094127 (2006).
- [30] J. Pollanen, K. Shirer, S. Blinstein, J. P. Davis, H. Choi, T. M. Lippman, L. B. Lurio, and W. P. Halperin, *J. Non-Crystalline Solids* **354**, 4668 (2008).
- [31] F. Souris, A. D. Fefferman, H. J. Maris, V. Dauvois, P. Jean-Baptiste, J. R. Beamish, and S. Balibar, *Phys. Rev. B* **90**, 180103(R) (2014).
- [32] Y. Vekhov, W. J. Mullin, and R. B. Hallock, *Phys. Rev. Lett.* **113**, 035302 (2014).
- [33] H. Matsuda, A. Ochi, R. Isozaki, R. Nomura, and Y. Okuda, *Low Temp. Phys.* **39**, 780 (2013). (*Fiz. Niz. Temp.* **39**, 1006 (2013).)
- [34] J. P. Sethna, K. A. Dahmen, and C. R. Myers, *Nature (London)*, **410**, 242 (2001).
- [35] See Supplemental Material at <http://link.aps.org/supplemental/XXX> for a movie of crystallization of <sup>4</sup>He in 96% aerogel by cooling shown in Fig. 1.
- [36] E. R. Grilly, *J. Low Temp. Phys.* **11**, 33 (1973).
- [37] A. M. Zimmerman, M. G. Specht, D. Ginzburg, J. Pollanen, J. I. A. Li, C. A. Collett, W. J. Gannon, and W. P. Halperin, *J. Low Temp. Phys.* **171**, 745 (2013).
- [38] S. G. Söyler, A. B. Kuklov, L. Pollet, N. V. Prokof'ev, and B. V. Svistunov, *Phys. Rev. Lett.* **103**, 175301 (2009).
- [39] T. Takahashi, H. Minezaki, A. Suzuki, K. Obara, K. Itaka, R. Nomura, and Y. Okuda, *Phys. Rev. E* **93**, 052806 (2016).
- [40] M. Boninsegni, A. B. Kuklov, L. Pollet, N.V. Prokof'ev,

- B. V. Svistunov, and M. Troyer, Phys. Rev. Lett. **99**, 035301 (2007).
- [41] F. Tsuruoka and Y. Hiki, Phys. Rev. B **20**, 2702 (1979).
- [42] A. Haziot, A. D. Fefferman, J. R. Beamish, and S. Balibar, Phys. Rev. B **87**, 060509(R) (2013).
- [43] J. Day, T. Herman, and J. Beamish, Phys. Rev. Lett. **95**, 035301 (2005).
- [44] J. Day and J. Beamish, Phys. Rev. Lett. **96**, 105304 (2006).
- [45] A. S. C. Rittner, W. Choi, E. J. Mueller, and J. D. Reppy, Phys. Rev. B **80**, 224516 (2009).